Calibrating the single-wall carbon nanotube resonance Raman intensity by high resolution transmission electron microscopy for a spectroscopy-based diameter distribution determination

P. B. C. Pesce,[1,a)] P. T. Araujo,[1] P. Nikolaev,[2,b)] S. K. Doorn,[3] K. Hata,[4] R. Saito,[5] M. S. Dresselhaus,[6] and A. Jorio[1,7]
[1]*Departamento de Física, Universidade Federal de Minas Gerais, 30123-970 Belo Horizonte, Brazil*
[2]*ERC Inc./NASA Johnson Space Center, Mail Stop ES-4, P.O. Box 58561, Houston, Texas 77258, USA*
[3]*Chemistry Division, Los Alamos National Laboratory, Los Alamos, New Mexico 87545, USA*
[4]*Nanotube Research Center, National Institute of Advanced Industrial Science and Technology (AIST), Tsukuba, 305-8565, Japan*
[5]*Department of Physics, Tohoku University, Sendai 980-8578, Japan*
[6]*Department of Physics and Department of Electrical Engineering and Computer Science, Massachusetts Institute of Technology, Cambridge, Massachusetts 02139, USA*
[7]*Divisão de Metrologia de Materiais, Instituto Nacional de Metrologia, Normalização e Qualidade Industrial (INMETRO), Duque de Caxias, 25250-020 RJ, Brazil*

(Received 18 November 2009; accepted 28 December 2009; published online 5 February 2010)

We study a single-wall carbon nanotube (SWNT) sample grown by water-assisted chemical vapor deposition with both resonance Raman scattering (RRS) and high resolution transmission electron microscopy. High resolution transmission electron microscopy measurements of 395 SWNTs determined the diameter distribution of the sample, allowing us to calibrate an RRS radial breathing mode (RBM) map obtained with 51 laser excitation energies from 1.26 to 1.73 eV. Thus, we determined the diameter dependence of the RRS RBM cross-section, which in turn allows the determination of the diameter distribution of any SWNT sample by measuring the RBM Raman signal. © *2010 American Institute of Physics*. [doi:10.1063/1.3297904]

Single-wall carbon nanotube (SWNT) samples usually consist of many different tube species, each characterized by a pair of indices (n,m), or equivalently by their diameter and chiral angle (d_t,θ).[1] Resonance Raman scattering (RRS) is an intensively used characterization method for SWNTs. Of particular interest is the radial breathing mode (RBM) feature in the RRS spectra, since each RBM peak can be assigned to a distinct (n,m) species.[1] The RRS RBM intensity depends on its cross-section times the number of scatterers, so the RRS RBM signal can be used to determine the relative population of each SWNT species. However, despite several theoretical[2–5] and experimental[6–12] efforts, a model-independent study of how the RRS RBM intensity varies with (n,m) is still needed. Here, we show that by combining RRS and high resolution transmission electron microscopy (HRTEM) measurements on the same sample, we can determine the RRS RBM cross-section, allowing us to obtain the d_t distribution of any SWNT sample via RRS RBM measurements.

The sample studied here was produced by water-assisted chemical vapor deposition ("super-growth"), yielding a vertical forest of nearly isolated, high quality SWNTs.[12–16] Its wide d_t distribution—1 to 6 nm, as established here—along with its high quality SWNTs make this an ideal sample for the present study. 51 RRS spectra were obtained from the as-grown sample, as previously reported.[12–15] These RBM spectra have already been extensively analyzed with respect to their resonance energies[12,14,15] and their adherence to the $\omega_{\mathrm{RBM}}=227/d_t$ cm^{-1} nm relation,[13] and they are now ready for an accurate intensity analysis. For each laser line, the nonresonant, integrated intensity of the two tylenol Raman peaks at 151 cm^{-1} and 213 cm^{-1} were used as intensity standards for the SWNT spectrum taken with the same laser excitation energy. In this way, the ν^4 Raman intensity dependence as well as the instrument response were accounted for.

HRTEM imaging was done using a JEOL 2000 FX instrument equipped with a LaB_6 gun, operating at a 160 kV acceleration voltage. Images were recorded with a 4 Megapixel Gatan charge-coupled device at a 250 000× magnification. HRTEM magnification factors were calibrated at 600 000× and above by determining the gold lattice parameters, at 400 000× by the graphite lattice spacing, and down to 250 000× by the dimensions of multiwall carbon nanotubes. The calibration at 250 000× was deemed accurate to 1.5%. The HRTEM sample was prepared by placing several very small particles of dry, as-grown carbon nanotubes on a holey carbon transmission electron microscopy grid (EMS 200 mesh copper grid) supported on a piece of tissue, and wetted with a drop of methanol.[17,18]

Homemade software was used to superimpose circles onto HRTEM images, adjust their diameters and positions until the best fit was achieved and the diameter was then determined. The white circles in Fig. 1(a) are the best fits for seven SWNTs present in this image. Nanotubes with noncircular cross-sections were excluded from the analysis. Figure 1(b) shows the experimentally obtained d_t distribution, fitted by the sum of two log-normal distributions,[19] obtained by measuring 395 SWNTs in this fashion. We assumed that SWNTs of different chiral angles are equally abundant for this growth process. Even if the assumption of chirality-independent growth is not correct, any under- (over-) estimation of the population of tubes with a certain chiral

a)Electronic mail: pedrop@fisica.ufmg.br.
b)Present address: Sungkyunkwan University, Suwon, Republic of Korea.

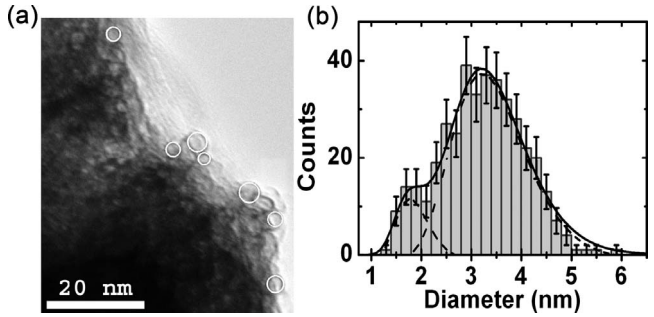

FIG. 1. (a) HRTEM image of the SWNT sample. The white circles represent circular fittings to determine the d_t. (b) Diameter distribution of the SWNT sample measured from HRTEM images, with a binning of 0.2 nm. Dashed lines are two log-normal distributions (f_1, f_2), defined as $f_i = A_i/(d_t\sigma_i) \times \exp[-\ln^2(d_t/\bar{d}_i)/(2\sigma_i^2)]$. The solid line is the sum of f_1 and f_2. Here, $A_1(A_2)=4(28)$, $\bar{d}_1(\bar{d}_2)=1.84(3.38)$ nm, $\sigma_1(\sigma_2)=0.183(0.223)$.

angle is compensated by an over-(under-) estimation of the RRS RBM cross-section dependence on θ. Therefore, its d_t dependence and consequent d_t distribution determination will still be correct. Accepting this assumption, the relative population of the SWNTs must scale as the d_t distribution times $1/d_t$, since the number of different (n,m) species of a given diameter scales linearly with d_t. Also, chiral SWNTs are twice as populous as achiral ones, as there are both right-handed and left-handed isomers.

Figure 2(a) shows the intensity calibrated experimental RRS map. Each nanotube in the sample contributes to the RBM RRS spectra with a Lorentzian line shape, whose total integrated area $(I^{E_L}_{(n,m)})$ for the Stokes process at a given excitation laser energy (E_L) is given by:[11,12]

$$I^{E_L}_{(n,m)} = \left| \frac{\mathcal{M}}{(E_L - E_{ii} + i\gamma)(E_L - E_{ph} - E_{ii} + i\gamma)} \right|^2, \quad (1)$$

where $E_{ph}=\hbar\omega_{RBM}$ is the energy of the RBM phonon, E_{ii} is the energy corresponding to the i-th excitonic transition, γ is the resonance window width and $\mathcal{M}$ represents the matrix elements for the Raman scattering by one RBM phonon of the (n,m) nanotube. Since each spectrum $(S_{(\omega,E_L)},)$ is the sum of the individual contributions of all SWNTs, it can be written as

TABLE I. Fitted parameters $\mathcal{M}_i$ and γ_i for metallic $(M: 2n+m \bmod 3=0)$, semiconductor type 1 $(S_1: 2n+m \bmod 3=1)$ and type 2 $(S_2: 2n+m \bmod 3=2)$ tubes. These parameters are to be used in Eq. (3) with d_t in nanometers, yielding $\mathcal{M}$ in arbitrary units and γ in milli-electron volts.

Type	$\mathcal{M}_A$	$\mathcal{M}_B$	$\mathcal{M}_C$	γ_A	γ_B	γ_C
M	1.68	0.52	5.54	23.03	48.84	1.03
S_1	−19.62	29.35	4.23	−3.45	65.10	7.22
S_2	−1.83	3.72	1.61	−10.12	42.56	−6.84

$$S_{(\omega,E_L)} = \sum_{n,m} \left[\mathrm{Pop}_{(n,m)} I^{E_L}_{(n,m)} \frac{\Gamma/2}{(\omega - \omega_{RBM})^2 + (\Gamma/2)^2} \right], \quad (2)$$

where $\mathrm{Pop}_{(n,m)}$ is the population of the (n,m) nanotube species, $\Gamma=3$ cm^{-1} is the experimental average value for the full width at half maximum intensity of the tube's RBM Lorentzian, ω_{RBM} is the frequency of its RBM and ω is the Raman shift.

The values for E_{ii} and ω_{RBM} were determined experimentally.[14] $\mathcal{M}$ and γ were found by fitting the experimental RBM RRS map with Eq. (2) using the functions

$$\mathcal{M} = \left[\mathcal{M}_A + \frac{\mathcal{M}_B}{d_t} + \frac{\mathcal{M}_C \cos(3\theta)}{d_t^2} \right]^2,$$

$$\gamma = \gamma_A + \frac{\gamma_B}{d_t} + \frac{\gamma_C \cos(3\theta)}{d_t^2}, \quad (3)$$

where $\mathcal{M}_i$ and $\gamma_i (i=A,B,C)$ are adjustable parameters. The best values for $\mathcal{M}_i$ and γ_i, considering the excitonic transitions E^S_{22} and the lower branch of E^M_{11} are listed in Table I for d_t in nanometers, γ in milli-electron volts, and $\mathcal{M}$ in arbitrary units.

Using these values in Eq. (2), we obtain the modeled RRS map shown in Fig. 2(b). Figure 2(c) shows the absolute value of the subtraction between the experimental and modeled maps. The overall low intensity of the features in Fig. 2(c) shows that the functionals chosen for $\mathcal{M}$ and γ are representative of their experimental behavior. A close inspection of the experimental RRS map shows some low intensity features associated with cross-polarized transitions (E^S_{12}) and

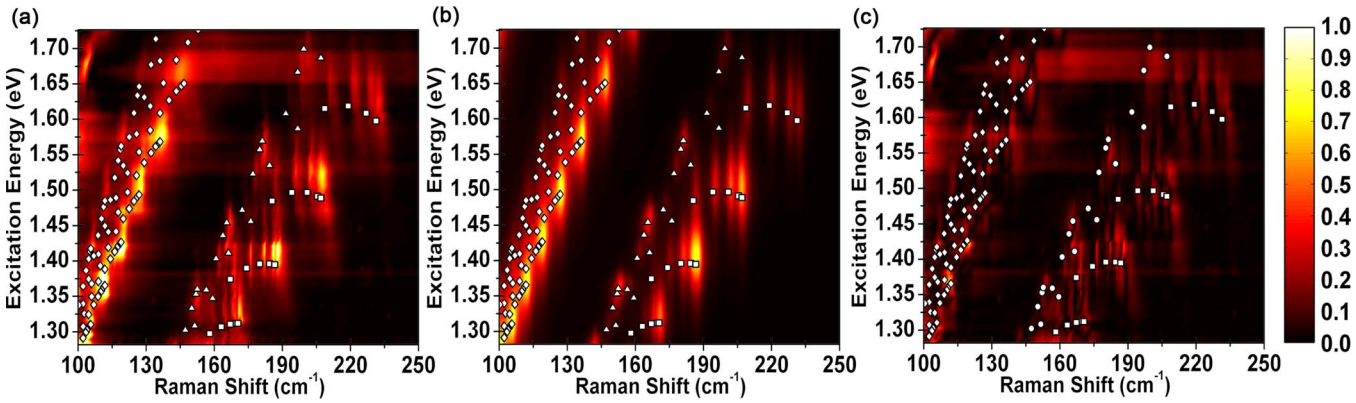

FIG. 2. (Color online) RBM RRS maps. (a) An experimental map. Intensity calibration was made by measuring a standard tylenol sample. (b) A modeled map obtained by using Eq. (2) at the same excitation energies range as (a). (c) Absolute value of the subtraction of the experimental (a) and modeled (b) maps. Symbols indicate the transition energies and ω_{RBM} for different SWNTs: diamonds for E^M_{11}, squares for $E^{S_1}_{22}$, and triangles for $E^{S_2}_{22}$. The color bar scale is the same for all three maps.

the RBM overtone. For our purposes, it is safe to ignore these features, since their total contribution to the RRS map is less than 4%.

At this point, the RRS RBM cross-section dependence on (n,m) is established for E_{22}^{S} and E_{11}^{M} for the "supergrowth" sample and these results can now be extended to the analysis of other samples. In order to determine the diameter distribution of a SWNT sample from RRS, one needs to know the relative RRS RBM intensity for each tube in the sample, which includes knowledge of E_{ii}, E_{ph}, $\mathcal{M}$, and γ. E_{ph} and E_{ii} are obtained from the literature for a wide variety of samples,[13,15] while $\mathcal{M}$ and γ are given here by Eq. (3). Comparison with the relative intensity ratios experimentally obtained yields the sample's d_t distribution. A user-friendly recipe for obtaining the d_t distribution from RBM RRS spectra is given in Ref. 20, along with a MatLab program for simulating RRS RBM spectra. While this procedure remains assumption-dependent for determination of the relative population of individual (n,m) species, it is assumption-independent for the d_t distribution. Though the values of $\mathcal{M}$ and γ may vary from sample to sample,[7] the procedure described here is certainly more accurate than a direct RBM Raman intensity analysis.

Comparison of Eq. (3) with published calculations[2–4] shows qualitative agreement for both γ and $\mathcal{M}$, that is, they both increase as the d_t decreases and the family patterns can be easily recognized on a plot of γ or $\mathcal{M}$ versus d_t. A quantitative comparison with Ref. 2 shows an underestimation of ≈ 40 meV for γ^{M} and of ≈ 15 meV for γ^{S_1}. Also, we find a steeper dependence of $\mathcal{M}^{S_1}$ on d_t than Ref. 3. A more detailed discussion is given in Ref. 20.

In summary, the diameter distribution of a pristine SWNT sample was determined by HRTEM and this result was compared with the RBM RRS map of the same sample. Under the assumption of equally distributed chiral angles, the RRS RBM cross-section of the SWNTs was determined and it was seen that it can be well represented by a simple empirical formula. The RBM intensity can now be used in the inverse process to yield the sample's diameter distribution. A user-friendly recipe for this procedure is given in Ref. 20, along with a comparative analysis of our experimental values with theoretical[2,3] calculations.

We thank J. S. Park, who kindly supplied us with additional data for the comparative analysis in Ref. 20. Brazilian authors acknowledge MCT-CNPq (Brazil) and AFOSR/SOARD (USA) (Award No. FA9550-08-1-236). P.N. acknowledges NASA under Contract No. NNJ05HI05C. S.K.D. acknowledges LANL LDRD program (USA). R.S. acknowledges NEXT (Grant No. 20241023). M.S.D. acknowledges NSF (Grant No. DMR-07-04197).

[1] A. Jorio, M. S. Dresselhaus, and G. Dresselhaus, *Carbon Nanotubes: Advanced Topics in Synthesis, Properties, and Applications, Topics in Applied Physics* (Springer, Berlin, 2008), Vol. 111.
[2] J. S. Park, Y. Oyama, R. Saito, W. Izumida, J. Jiang, K. Sato, C. Fantini, A. Jorio, G. Dresselhaus, and M. S. Dresselhaus, Phys. Rev. B **74**, 165414 (2006).
[3] J. Jiang, R. Saito, K. Sato, J. S. Park, G. G. Samsonidze, A. Jorio, G. Dresselhaus, and M. S. Dresselhaus, Phys. Rev. B **75**, 035405 (2007).
[4] S. V. Goupalov, B. C. Satishkumar, and S. K. Doorn, Phys. Rev. B **73**, 115401 (2006).
[5] M. Machón, S. Reich, H. Telg, J. Maultzsch, P. Ordejón, and C. Thomsen, Phys. Rev. B **71**, 035416 (2005).
[6] Z. L. Luo, F. Papadimitrakopoulos, and S. K. Doorn, Appl. Phys. Lett. **88**, 073110 (2006).
[7] Z. L. Luo, F. Papadimitrakopoulos, and S. K. Doorn, Phys. Rev. B **77**, 035421 (2008).
[8] T. Okazaki, T. Saito, K. Matsuura, S. Ohshima, M. Yumura, Y. Oyama, R. Saito, and S. Iijima, Chem. Phys. Lett. **420**, 286 (2006).
[9] A. Jorio, A. P. Santos, H. B. Ribeiro, C. Fantini, M. Souza, J. P. M. Vieira, C. A. Furtado, J. Jiang, R. Saito, L. Balzano, D. E. Resasco, and M. A. Pimenta, Phys. Rev. B **72**, 075207 (2005).
[10] H. Telg, J. Maultzsch, S. Reich, and C. Thomsen, Phys. Rev. B **74**, 115415 (2006).
[11] A. Jorio, C. Fantini, M. A. Pimenta, R. B. Capaz, G. G. Samsonidze, G. Dresselhaus, M. S. Dresselhaus, J. Jiang, N. Kobayashi, A. Grüneis, and R. Saito, Phys. Rev. B **71**, 075401 (2005).
[12] S. K. Doorn, P. T. Araujo, K. Hata, and A. Jorio, Phys. Rev. B **78**, 165408 (2008).
[13] P. T. Araujo, I. O. Maciel, P. B. C. Pesce, M. A. Pimenta, S. K. Doorn, H. Qian, A. Hartschuh, M. Steiner, L. Grigorian, K. Hata, and A. Jorio, Phys. Rev. B **77**, 241403 (2008).
[14] P. T. Araujo and A. Jorio, Phys. Status Solidi B **245**, 2201 (2008).
[15] P. T. Araujo, A. Jorio, M. S. Dresselhaus, K. Sato, and R. Saito, Phys. Rev. Lett. **103**, 146802 (2009).
[16] K. Hata, D. N. Futaba, K. Mizuno, T. Namai, M. Yumura, and S. Iijima, Science **306**, 1362 (2004).
[17] A. Thess, R. Lee, P. Nikolaev, H. J. Dai, P. Petit, J. Robert, C. H. Xu, Y. H. Lee, S. G. Kim, A. G. Rinzler, D. T. Colbert, G. E. Scuseria, D. Tomanek, J. E. Fischer, and R. E. Smalley, Science **273**, 483 (1996).
[18] P. Nikolaev, A. Thess, A. G. Rinzler, D. T. Colbert, and R. E. Smalley, Chem. Phys. Lett. **266**, 422 (1997).
[19] L. B. Kiss, J. Söderlund, G. A. Niklasson, and C. G. Granqvist, Nanotechnology **10**, 25 (1999).
[20] See supplementary material at http://dx.doi.org/10.1063/1.3297904 for our recipe to determining the d_t distribution from RRS RBM measurements, including a MatLab program. Also, we present a detailed discussion of the agreement of our $\mathcal{M}$ and γ and the theoretical calculations of Refs. 2 and 3.